

Research Article

Core-Shell Structure of Gold Nanoparticles with Inositol Hexaphosphate Nanohybrids for Label-Free and Rapid Detection by SERS Nanotechnology

Andreas H. H. Mevold,¹ Jin-Yuan Liu,¹ Li-Ying Huang,¹
Hung-Liang Liao,¹ Ming-Chien Yang,¹ Tzu-Yi Chan,² Kuan-Syun Wang,²
Juen-Kai Wang,^{3,4} Yuh-Lin Wang,^{4,5} and Ting-Yu Liu²

¹Department of Materials Science and Engineering, National Taiwan University of Science and Technology, Taipei 106, Taiwan

²Department of Materials Engineering, Ming Chi University of Technology, New Taipei City 24301, Taiwan

³Center for Condensed Matter Sciences, National Taiwan University, Taipei 10617, Taiwan

⁴Institute of Atomic and Molecular Sciences, Academia Sinica, Taipei 10617, Taiwan

⁵Department of Physics, National Taiwan University, Taipei 10617, Taiwan

Correspondence should be addressed to Ming-Chien Yang; myang@mail.ntust.edu.tw and Ting-Yu Liu; tyliu0322@gmail.com

Received 5 February 2015; Accepted 16 March 2015

Academic Editor: Ping Yang

Copyright © 2015 Andreas H. H. Mevold et al. This is an open access article distributed under the Creative Commons Attribution License, which permits unrestricted use, distribution, and reproduction in any medium, provided the original work is properly cited.

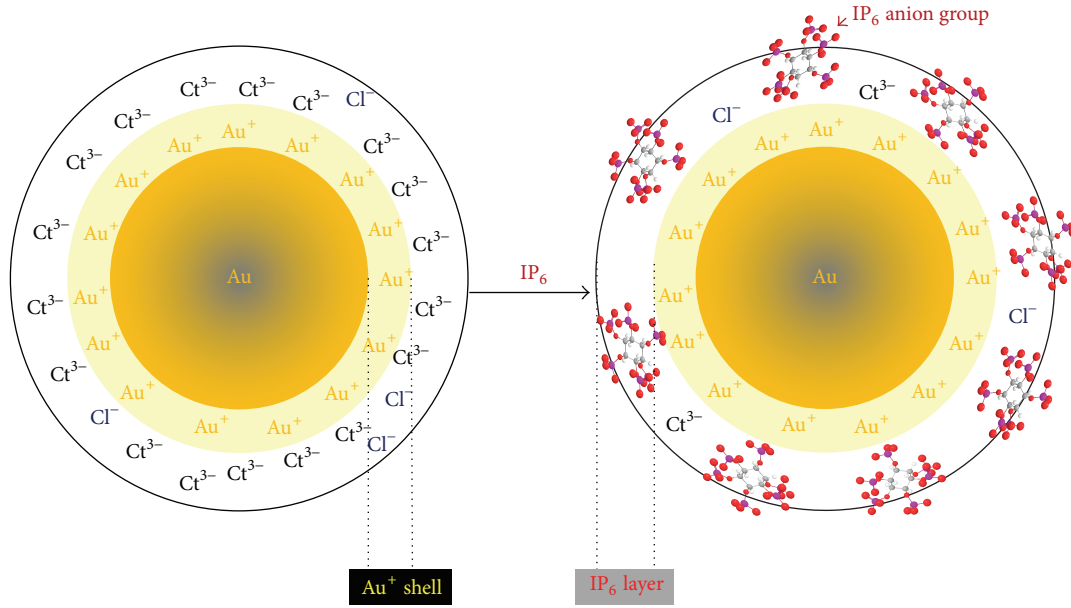
Gold nanoparticles bound with inositol hexaphosphate (IP₆) (AuNPs/IP₆) were prepared by *in situ* reduction of various concentrations of IP₆ (0–320 μM) through modified Frens method for surface-enhanced Raman scattering (SERS) detection. The resultant AuNPs/IP₆ were subject to characterization including UV/Vis spectroscopy, transmission electron microscopy (TEM), dynamic light scattering (DLS), zeta potential, and X-ray photoelectron spectroscopy (XPS). The results showed that AuNPs with 65 μM of IP₆ would result in a core AuNPs-shell (IP₆ layer) structure, which exhibited the strongest SERS signal, due to the “hot spot effect” generated from the 1–2 nm interparticle gaps of AuNPs/IP₆ nanohybrids (ionic interaction of IP₆ and Au⁺). Furthermore, the reaction kinetics of Au and IP₆ were also investigated in this work. Higher concentration of IP₆ (190 and 260 μM) will make AuNPs become irregularly shaped, because IP₆ is a basic salt and served as a pH mediator. The morphology and distribution of AuNPs were greatly improved by addition of 65 μM of IP₆. This novel AuNPs/IP₆ nanohybrid showed great stability and Raman enhancement. It is promising in the application of rapid and label-free biological detection of bacteria or tumor cells.

1. Introduction

Raman scattering was discovered by C. V. Raman in 1928 and SERS technology was developed by Fleischman and others in 1974 [1]. In recent years, SERS has been employed for label-free sensing of bacteria such as *Escherichia coli* (*E. coli*) or various molecules, exploiting its tremendous enhancement of the Raman signal. Gold and silver nanoparticles are widely used in this field [2–4], because they produce localized surface plasma resonance (LSPR), which can increase the intensity of the Raman signal by at least 10⁹. Gold and silver nanoparticles have unique optical, electrical, and magnetic properties because of their particle size and morphology.

Therefore controlling the size and morphology is important when synthesizing nanoparticles [5–7]. Gold and silver nanoparticles (NPs) increase Raman signal under specific frequency because LSPR produces electromagnetic field, which will increase the Raman signal of the absorbed molecule. If we further limit the space between these metal nanoparticles at 1–2 nm, it will produce “hot spot” effect, which will further increase the intensity of the SERS signals [2–4]. Therefore these materials showed promising potential in the application of SERS [8, 9] and biosensing [10, 11].

Inositol hexaphosphate (IP₆) is known as phytic acid sodium salt, a naturally derived material. It could be used to prepare oral cleansing agent, water treatment agent, food



SCHEME 1: Schematic figure of core-shell structure of AuNPs/IP₆ nano hybrids.

additive, and so on because of its nontoxic and natural properties [12]. The structure of IP₆ contains six phosphate acid groups (negatively charged) which are able to link with metal particles and have good absorption capability. Therefore we will employ IP₆ as a tunable cross linker (or spacer) to obtain AuNPs with a distance between each other at 1-2 nm.

In this work, AuNPs were produced by a procedure developed by Frens et al. in 1973 using sodium citrate to reduce HAuCl₄ to produce monodispersed AuNPs. In this present work, IP₆ was added during the reduction procedure and its adsorption onto the AuNPs led to the final product AuNPs/IP₆. The final product will be further tested in the application of SERS for detecting microorganism *Staphylococcus aureus*.

2. Experimental Procedure

2.1. Materials. Inositol hexaphosphate (IP₆), sodium citrate dihydrate (Na₃Ct·2H₂O), hydrogen tetrachloroaurate (III) trihydrate (HAuCl₄·3H₂O), and sodium hydroxide (NaOH) were purchased from Sigma-Aldrich. Nitric acid (HNO₃) was purchased from Scharlau, Spain. Silicon oil was purchased from Choneye Pure Chemical. Luria-Bertani (LB) broth was purchased from Difco. Bacteriological agar was obtained from Oxoid Ltd., UK. All glassware was cleaned with aqua-regia and rinsed with deionized water prior to the experiment. *Staphylococcus aureus* was obtained from Super Laboratory Co., Taiwan.

2.2. Synthesis of Gold Nanoparticles. The gold nanoparticles were synthesized on the basis of the method developed by Frens et al. Table 1 lists the solution for preparing AuNPs/IP₆ by mixing 0.01% HAuCl₄ with 1.0 mM IP₆ stock solution. When the solutions were boiling for 10 min, 3.5 mL of 1%

TABLE 1: The solution compositions for the preparation of HAuCl₄/IP₆.

Sample	0.01% HAuCl ₄ (mL)	1 mM IP ₆ (mL)	H ₂ O (mL)
A0	70	0	35
A1	70	2.8	32.2
A2	70	7	28
A3	70	14	21
A4	70	21	14
A5	70	28	7
A6	70	35	0

sodium citrate was then added drop wisely. During the reaction, the color of the solution turned from light yellow color to brick red color. The reaction completed when the color no longer changed and the final solution result was referred to here as gold colloids. The samples of HAuCl₄/IP₆ solutions were analyzed using TEM and DLS as described in the following section. Scheme 1 depicts the core-shell structure of AuNPs/IP₆ nano hybrids.

2.3. Reaction Time for HAuCl₄/IP₆ Solutions. The reaction time of the gold colloids is the time required for the reaction of HAuCl₄ and IP₆ to be completed when the color no longer changes. The exhausted time for HAuCl₄ was monitored according to the way developed by Ji et al. [13]. Temporal evolution of HAuCl₄ was obtained by measuring the pH 10 times before the exhaustion of HAuCl₄ with IP₆ and initial reaction rate was also obtained.

2.4. TEM of the AuNPs of the Gold Colloids. An aliquot of 5 μL of the gold colloids described in Section 2.2 was placed on the copper grid and dried in the autoclave. Afterwards,

TABLE 2: Wavelength and absorbance of AuNPs/IP₆ in different concentrations of IP₆.

Sample	[IP ₆] (μM)	Wavelength 1 (nm)	Wavelength 2 (nm)	Absorbance 1	Absorbance 2
A0	0	525	—	0.63	—
A1	26	524	—	0.66	—
A2	65	526	—	0.67	—
A3	130	534	—	0.59	—
A4	190	549	648	0.48	0.49
A5	260	549	725	0.35	0.32
A6	320	534	655	0.34	0.21

they were placed in a copper grid box and analyzed using TEM (H7650, Hitachi, Japan) for the size distribution (diameter) and morphology of AuNPs.

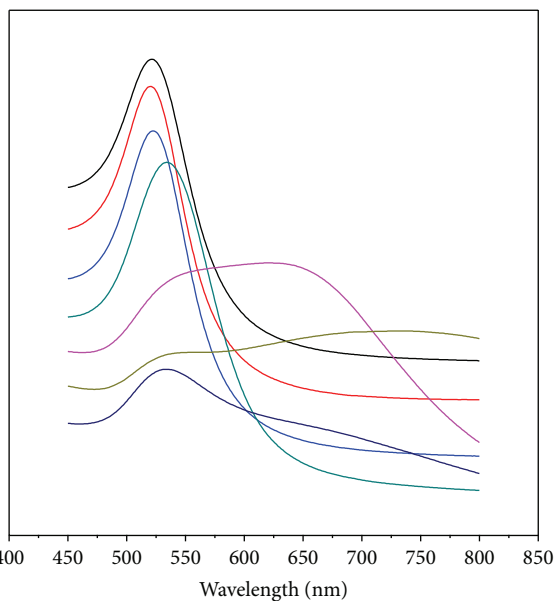
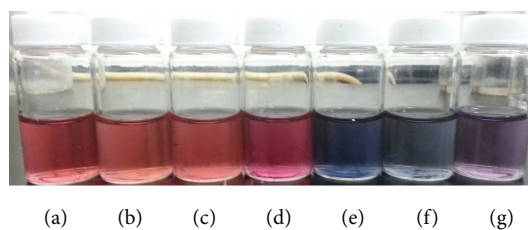
2.5. Dynamic Light Scattering (DLS) of the Gold Colloids. The gold colloids (1 mL) were placed in a DLS cuvette followed by sonicating for 5 s before DLS (Nano ZS, Malvern Instruments, UK) analysis. Each sample was analyzed 3 times.

2.6. SERS Measurements of AuNPs/IP₆. Raman microscope (HR800, Horiba, Japan) with He-Ne laser (632.8 nm) was used to detect the presence of *S. aureus* (ATCC 6538P). 50 μL of the varied AuNPs/IP₆ and 50 μL of *S. aureus* (1×10^5 cfu/mL grown for 18 h at 37°C) were placed in 1.5 mL microcentrifuge tubes and mixed well. Then 5 μL of each sample was dropped on the aluminum sheet. Raman spectra in the range of 600 and 900 cm^{-1} were evaluated for these 6 samples. Intensity of the Raman signal at 733 cm^{-1} (SERS signal from the cell wall of *S. aureus*) for the samples was further investigated, as shown in Figure 8.

2.7. Characterization Analysis of AuNPs/IP₆. The interaction between AuNPs and IP₆ samples were analyzed by X-ray photoelectron spectroscopy (XPS, VG ESCA Scientific, Theta Probe) and surface electric properties of AuNPs/IP₆ samples were analyzed by zeta potential analyzer (Nano S90, Malvern Instruments) as described below.

3. Results and Discussions

3.1. Characterization of AuNPs. LSPR wavelength and colors of solutions displayed different pattern of adsorption as shown in Figure 1. Gold colloids of various IP₆ concentrations displayed various colors (Figures 1(a)–1(g)). Solutions A0 to A2 displayed brick red color or high concentration of AuNPs, A3 exhibited purple red color, A4 and A5 displayed blue color, and A6 showed purple color. UV/Vis spectroscopy showed a strong single absorption peak of the AuNPs/IP₆ and absorbed wavelength of the major peak gradually increases (red-shift) from 525 nm (A0) to 534 nm (A3) (Table 2; Figures 1(a) to 1(c)), implying that the diameter of the spherical AuNPs was about 30 nm and the color of Au colloids is brick red. Moreover, the peaks of A1 and A3 were sharper than the peak of A0; thereby the morphology and diameter of AuNPs are more homogeneous than AuNPs



(a) 0 μM (e) 190 μM
 (b) 26 μM (f) 260 μM
 (c) 65 μM (g) 320 μM
 (d) 130 μM

(h)

FIGURE 1: Effect of IP₆ concentration on the color of AuNPs/IP₆ solutions. (a) A0, (b) A1, (c) A2, (d) A3, (e) A4, (f) A5, (g) A6, and (h) UV/Visible spectra.

without IP₆. Figures 1(e) and 1(f) showed 2 peaks and implied that AuNPs display anisotropic structures. The first peak with lower wavelength was fraction of transverse absorption and the second peak with higher wavelength was longitudinal absorption. Further analysis by TEM also confirmed that both of them are irregular shaped AuNPs.

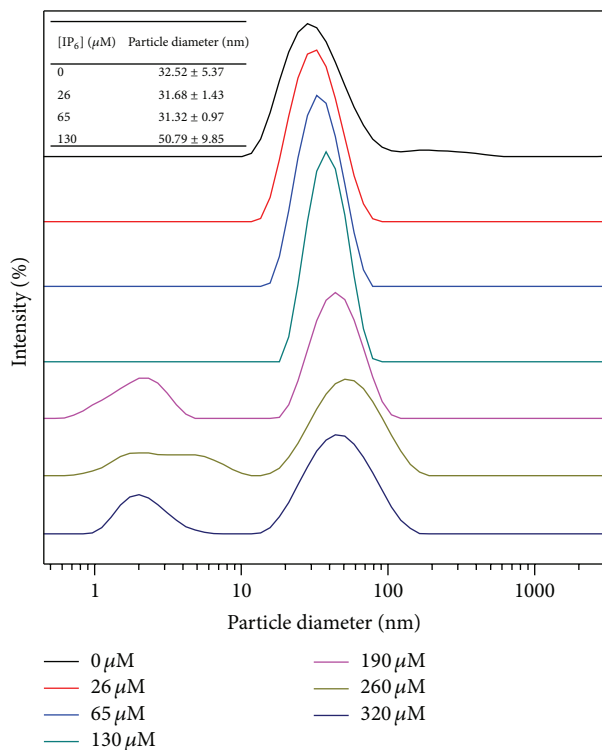


FIGURE 2: Effect of concentrations of IP₆ on the size distributions of AuNPs/IP₆.

TABLE 3: Dependence of exhausted time of H₂AuCl₄/IP₆ on the concentration of IP₆.

Sample	[IP ₆] (μM)	Exhausted time (min.)	pH
A1	26	12	3.51
A2	65	20	3.73
A3	130	30	4.42
A4	190	80	6.05
A5	260	150	7.29
A6	320	310	8.72

3.2. DLS Analysis of the Gold Colloids. DLS measurements of the particle diameter from A0, A1, and A2 were 32.52 ± 5.37 , 31.68 ± 1.43 , and 31.32 ± 0.97 nm, respectively (Figure 2). This result agreed with the results of UV/Vis spectra for being spherical shaped. Since the smallest standard deviation of the particle diameter was from A2, the AuNPs with $65 \mu\text{M}$ of IP₆ showed more uniform morphology and diameter as compared to the traditional process of thermal citrate reduction method without addition of IP₆.

3.3. TEM Analysis of the Gold Colloids. The IP₆ layer can clearly be observable in Figures 3(b) and 3(c), especially in Figure 3(c) for A2. There are two absorption peaks shown in samples A4 and A5 (Figures 1(e) and 1(f)); the second absorption peak was observed at 648 and 725 nm, respectively. This indicates that AuNPs/IP₆ formed irregular structures [14–16],

which was also observable in the TEM images (Figures 3(e) and 3(f)). There are many oval and prism shaped AuNPs. TEM and DLS results showed that the irregular nanoparticles were observed as the concentrations of IP₆ increased from $190 \mu\text{M}$ to $260 \mu\text{M}$. The morphology of AuNPs changed to spherical structures again when the concentrations of IP₆ reached $320 \mu\text{M}$, which displays a small second peak at 655 nm and just little irregular shaped AuNPs were found.

3.4. Exhausted Time and Initial Reaction Rate of Gold Colloids.

The reason why the morphology of AuNPs became irregularly shaped when the concentration of IP₆ reaches 190 and $260 \mu\text{M}$ was because IP₆ is a basic salt and served as a “pH mediator.” It can change the pH of auric acid solutions, leading to the growth of irregular shaped AuNPs. Higher concentration of IP₆ caused the pH of the solution to increase and $[\text{AuCl}_4]^-$ is converted to a less reactive $[\text{AuCl}_x(\text{OH})_{4-x}]^-$. Therefore at higher pH, $[\text{OH}^-]$ will increase and react with $[\text{AuCl}_4]^-$, forming a less reactive $[\text{AuCl}_x(\text{OH})_{4-x}]^-$ substance. Therefore higher concentration IP₆ will cause the exhausted time of H₂AuCl₄/IP₆ to increase. As shown in Figure 4 and Table 3, the exhausted time increased greatly with the addition of 190 and $260 \mu\text{M}$ of IP₆, as compared to the addition of the 26 – $130 \mu\text{M}$ of IP₆. The calculation method for temporal evolution curve of H₂AuCl₄ concentration used at least eight concentration points for each reaction into a Taylor expansion polynomial (average *R*-squared value for all reactions in Figure 4 is 98%) [17]. The formation of irregular shaped AuNPs is probably caused by the following: (1) AuCl under high concentration of IP₆ was not reactive enough to produce AuNPs and might go through nucleation twice to cause aggregation; (2) IP₆ attached to specific surface of Au seeds and induced AuCl to grow on the specific surface of Au seeds leading to the formation of irregular AuNPs.

Figure 5 shows that with the addition of 26 and $65 \mu\text{M}$ of IP₆, the initial reaction rate was much faster as compared to $0 \mu\text{M}$ of IP₆; therefore H₂AuCl₄ can be exhausted immediately to develop spherical shaped AuNPs. With the addition of 190 and $260 \mu\text{M}$ of IP₆, the initial reaction rate was slower than those of 0 – $130 \mu\text{M}$ of IP₆, because the reactivity of auric salt decreased with the increasing of pH of the solution [18, 19] due to increase of IP₆ concentration. With the addition of $320 \mu\text{M}$ of IP₆, the initial reaction rate was very low and the extremely slow reaction rate caused the formation of some spherical shaped AuNPs once again.

Figure 6 illustrates our hypotheses explaining the effect of IP₆ concentration on the morphology of AuNPs. 26 and $65 \mu\text{M}$ of IP₆ caused the reaction to develop faster as compared to formation of AuNPs without the addition of IP₆. With the addition of 190 and $260 \mu\text{M}$ of IP₆, the formation of AuNPs is slow along with formation of irregular shaped AuNPs as mentioned in Section 3.4. When the concentrations of IP₆ were increased to $320 \mu\text{M}$, some AuNPs spherical structures were formed (Figure 3(g)). This is because of extreme slow reaction rate causing Au seeds to form slowly and therefore there is less formation of second nucleation or aggregation of AuNPs.

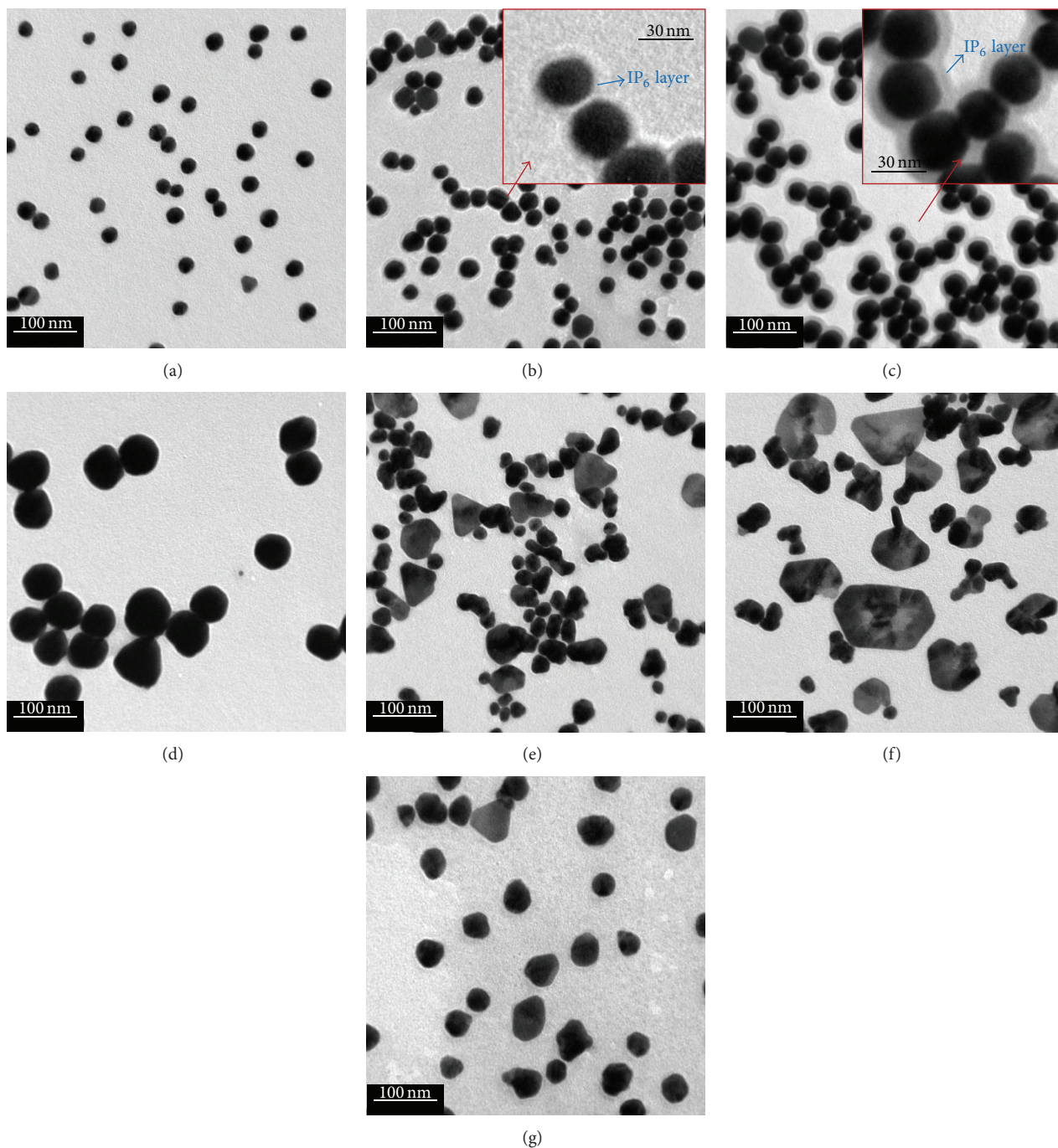


FIGURE 3: TEM images of AuNPs/IP₆ in different concentrations of IP₆: (a) 0 μM , (b) 26 μM , (c) 65 μM , (d) 130 μM , (e) 190 μM , (f) 260 μM , and (g) 320 μM .

3.5. SERS Application of AuNPs/IP₆. Figure 7 shows the SERS spectra of *S. aureus* using AuNPs/IP₆. The SERS peak at 733 cm^{-1} was from the cell wall of *S. aureus* and the strongest enhancement was observed for A2 as shown in Figure 7. Figure 7 also shows that A2 exhibits the strongest SERS intensity, which was 280040 ± 74600 and was about 40 times that of A0 (7705 ± 3295). Therefore the AuNPs reduced with the presence of 65 μM of IP₆ would enhance the SERS

signal more than that without the addition of IP₆. This is also confirmed with the TEM images in Figure 3, where the addition of 65 μM of IP₆ produced most visible IP₆ layer formed on the surface of AuNPs. This core-shell structure not only made AuNPs disperse well but also led to a specific distance of 1-2 nm between AuNPs. This is the reason why A2 greatly increased the intensity of the Raman signal by detecting *S. aureus*.

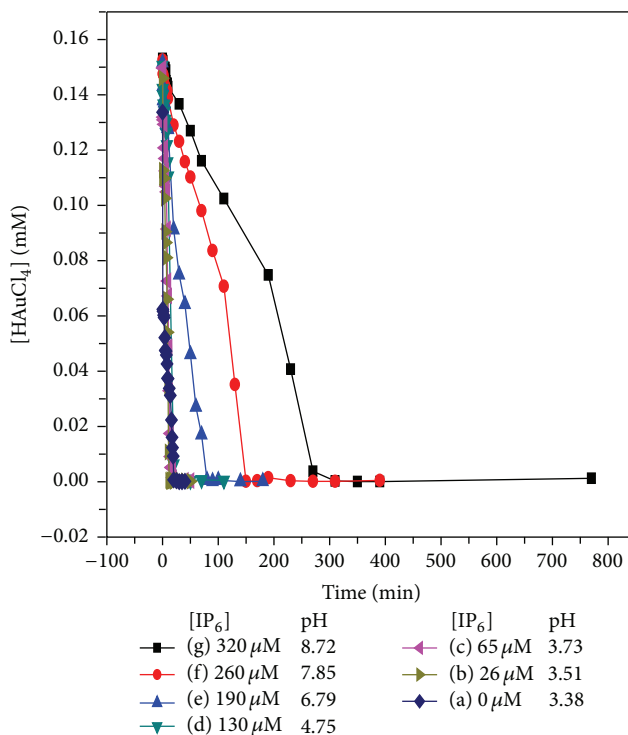


FIGURE 4: Temporal evolution of HAuCl_4 concentration for the reaction with different IP_6 concentrations as labeled.

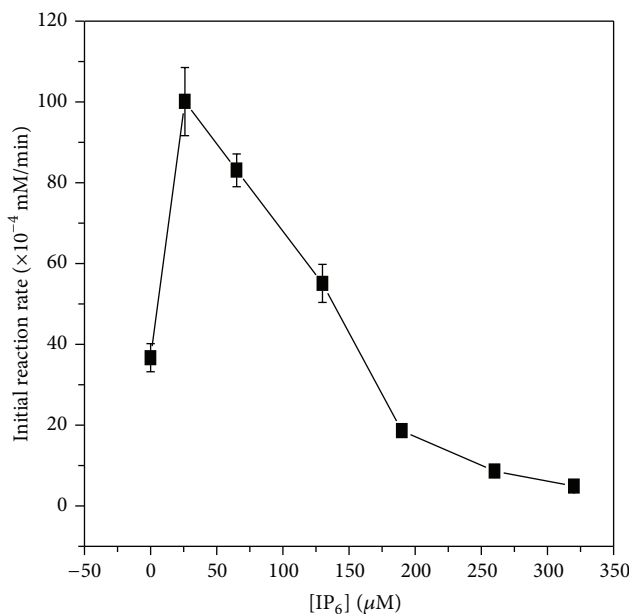


FIGURE 5: Effect of IP_6 concentration on the initial reaction rates of HAuCl_4 .

3.5.1. *Zeta Potential and XPS Analysis of AuNPs/IP₆*. The interaction between AuNPs and IP_6 was further investigated by zeta potential and XPS analysis, as shown in Figure 10. Figure 9 shows that the zeta potential decreased from -42.9 ± 2.15 to -54.83 ± 1.22 mV when the concentrations of IP_6 increased from 0 to 65 μM . Thus the negative charge on the

surface of AuNPs increased with increasing IP_6 concentrations and higher IP_6 will induce more IP_6 molecules absorbed on the surface of AuNPs. XPS analysis showed 0.4 eV and 0.3 eV binding energy shifting of $\text{Au}_{7/2}$ (84.5 to 84.9) and $\text{Au}_{5/2}$ (88.1 to 88.4) from 0 μM to 65 μM of IP_6 addition, respectively. This showed that IP_6 interacted with Au^+ NPs

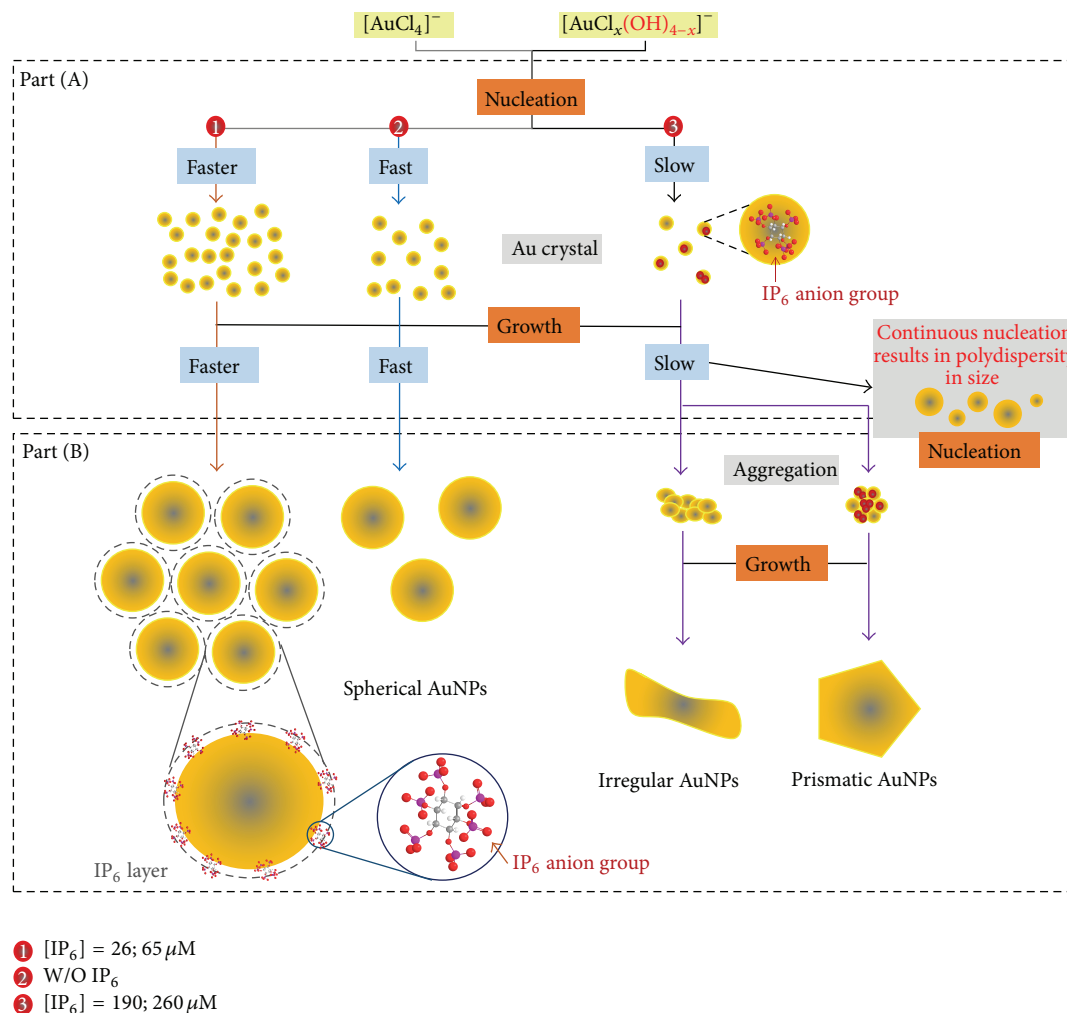


FIGURE 6: The mechanism of AuNPs formation with different IP_6 concentration.

by electrostatic force. Therefore, IP_6 definitely formed a layer on the surface of AuNPs with $65 \mu M$ of IP_6 . This layer not only controlled the interparticle gaps of AuNPs within 1-2 nm from each other but also produced huge “hot spots” effect which greatly increased the Raman intensity of the sample molecules.

Zeta potential and XPS analysis indicated that $65 \mu M$ of IP_6 was an ideal concentration leading to formation of IP_6 layer on the surface of AuNPs. The IP_6 layer not only kept AuNPs within a specific interparticle distance (1-2 nm) by ionic force, it also increased dispersion of AuNPs. On the other hand, irregular AuNPs or prismatic AuNPs formed with $190 \mu M$ and $260 \mu M$ of IP_6 . Thus in addition to improve the monodispersity of these anisotropic structures, irregular AuNPs can also be produced by adjusting the IP_6 concentration.

In summary, A2 showed more uniform morphology and diameter as compared to A0. A2 exhibited nanoscale interparticle gaps (1-2 nm) between AuNPs, thereby producing very huge “hot spots” effect, leading to greater enhancement

of SERS signal. This is a convenient way to fabricate well-dispersed AuNPs, which exhibited interparticle distance of $\sim 1-2$ nm, while providing excellent biocompatibility. Therefore, $65 \mu M$ of IP_6 bound to AuNPs has great potential for further industrial application of SERS biosensing of bacteria or cancer cells.

4. Conclusion

The core-shell structure of AuNPs/ IP_6 nanohybrids was successfully *in situ* synthesized by modified Frens method, which was applied in the rapid SERS detection of bacteria. In particular, by reducing $H[AuCl_4]$ in $65 \mu M$ of IP_6 , the morphology and distribution of AuNPs were greatly improved as compared to the AuNPs without IP_6 . Furthermore, AuNPs formed in $65 \mu M$ of IP_6 exhibited enormous “hot spots” effect, leading to greater enhancement of SERS signal. Thus, our works demonstrated a convenient way to fabricate well-dispersed AuNPs that can induce outstanding SERS enhancement that is applicable for label-free detection and biodetection of microbes and cancerous cells.

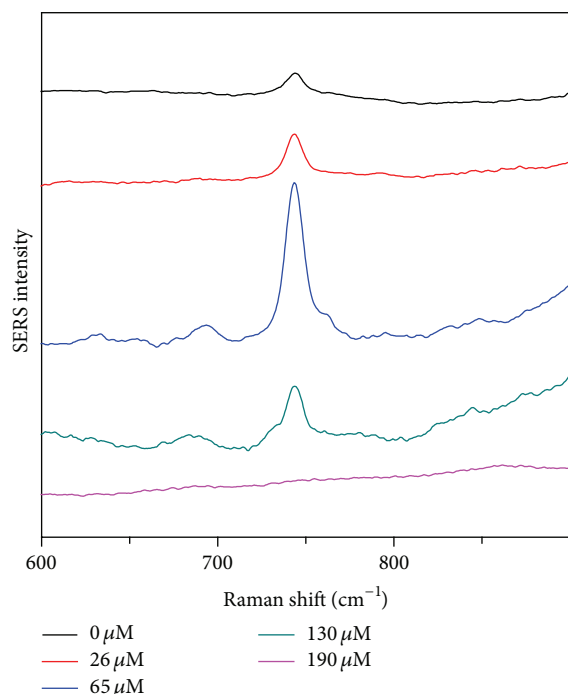


FIGURE 7: SERS spectra of *S. aureus* using different IP₆ concentration of AuNPs.

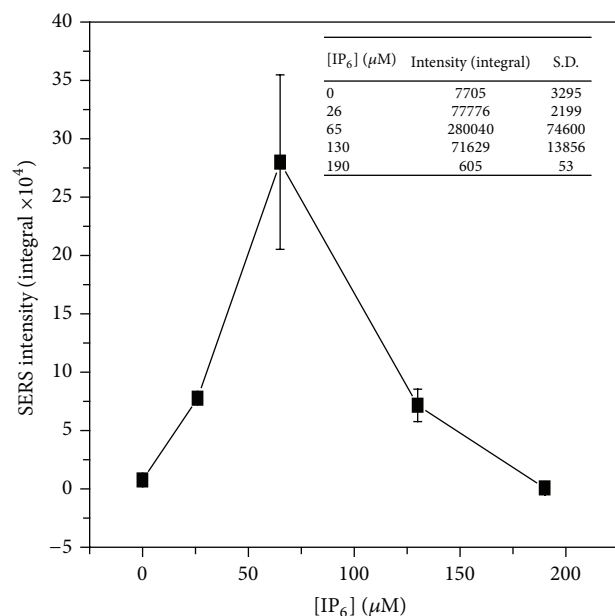


FIGURE 8: The effect of IP₆ concentration on the SERS intensity at 733 cm⁻¹ of *S. aureus*.

Conflict of Interests

The authors declare no competing financial interests.

Authors' Contribution

The paper was written by contributions of all authors. All authors have given approval for the final version of the paper.

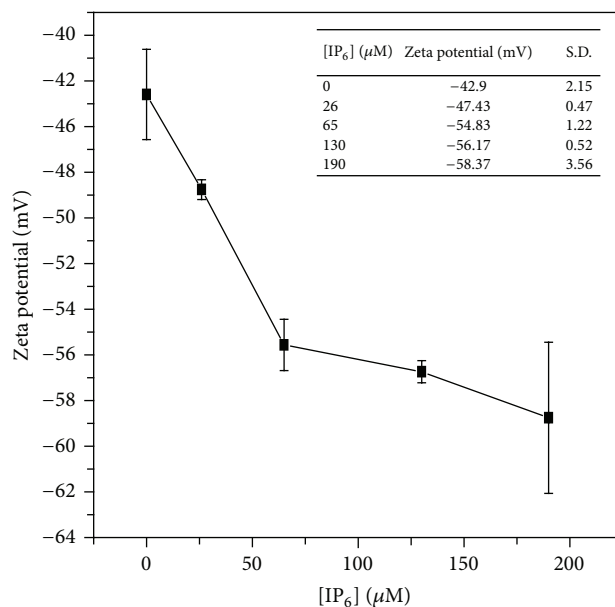


FIGURE 9: Effect of IP₆ concentration on the zeta potential of AuNPs/IP₆.

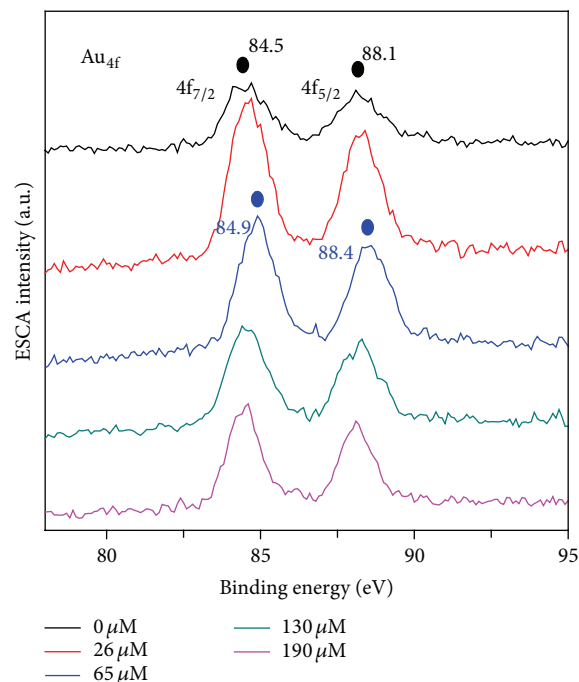


FIGURE 10: Effect of IP₆ concentration on the XPS spectra of AuNPs/IP₆.

Acknowledgments

This work was financially supported by Ministry of Science and Technology of Taiwan (MOST 103-2628-M-001-002 and MOST 103-2221-E-131-019). The authors also thank National Taiwan University for allowing them to use their TEM Lab in order to obtain TEM images for this experiment.

References

- [1] M. Fleischmann, P. J. Hendra, and A. J. McQuillan, "Raman spectra of pyridine adsorbed at a silver electrode," *Chemical Physics Letters*, vol. 26, no. 2, pp. 163–166, 1974.
- [2] E. Hao and G. C. Schatz, "Electromagnetic fields around silver nanoparticles and dimers," *Journal of Chemical Physics*, vol. 120, no. 1, pp. 357–366, 2004.
- [3] P. G. Etchegoin and E. C. le Ru, "A perspective on single molecule SERS: current status and future challenges," *Physical Chemistry Chemical Physics*, vol. 10, no. 40, pp. 6079–6089, 2008.
- [4] J. P. Camden, J. A. Dieringer, Y. Wang et al., "Probing the structure of single-molecule surface-enhanced Raman scattering hot spots," *Journal of the American Chemical Society*, vol. 130, no. 38, pp. 12616–12617, 2008.
- [5] N. R. Jana, L. Gearheart, and C. J. Murphy, "Seeding growth for size control of 5–40 nm diameter gold nanoparticles," *Langmuir*, vol. 17, no. 22, pp. 6782–6786, 2001.
- [6] L. Pei, K. Mori, and M. Adachi, "Formation process of two-dimensional networked gold nanowires by citrate reduction of AuCl₄⁻ and the shape stabilization," *Langmuir*, vol. 20, no. 18, pp. 7837–7843, 2004.
- [7] C. J. Murphy, A. M. Gole, S. E. Hunyadi, and C. J. Orendorff, "One-dimensional colloidal gold and silver nanostructures," *Inorganic Chemistry*, vol. 45, no. 19, pp. 7544–7554, 2006.
- [8] A. M. Michaels, J. Jiang, and L. Brus, "Ag nanocrystal junctions as the site for surface-enhanced Raman scattering of single rhodamine 6G molecules," *Journal of Physical Chemistry B*, vol. 104, no. 50, pp. 11965–11971, 2000.
- [9] L. L. Zhao, L. Jensen, and G. C. Schatz, "Surface-enhanced Raman scattering of pyrazine at the junction between two Ag₂₀ nanoclusters," *Nano Letters*, vol. 6, no. 6, pp. 1229–1234, 2006.
- [10] T. A. Taton, C. A. Mirkin, and R. L. Letsinger, "Scanometric DNA array detection with nanoparticle probes," *Science*, vol. 289, no. 5485, pp. 1757–1760, 2000.
- [11] A. G. Tkachenko, H. Xie, D. Coleman et al., "Multifunctional gold nanoparticle-peptide complexes for nuclear targeting," *Journal of the American Chemical Society*, vol. 125, no. 16, pp. 4700–4701, 2003.
- [12] X. Zhu, H. Yang, N. Wang et al., "A facile method for preparation of gold nanoparticles with high SERS efficiency in the presence of inositol hexaphosphate," *Journal of Colloid and Interface Science*, vol. 342, no. 2, pp. 571–574, 2010.
- [13] X. Ji, X. Song, J. Li, Y. Bai, W. Yang, and X. Peng, "Size control of gold nanocrystals in citrate reduction: the third role of citrate," *Journal of the American Chemical Society*, vol. 129, no. 45, pp. 13939–13948, 2007.
- [14] E. Hao, R. C. Bailey, G. C. Schatz, J. T. Hupp, and S. Li, "Synthesis and optical properties of 'Branched' gold nanocrystals," *Nano Letters*, vol. 4, no. 2, pp. 327–330, 2004.
- [15] C. Burda, X. Chen, R. Narayanan, and M. A. El-Sayed, "Chemistry and properties of nanocrystals of different shapes," *Chemical Reviews*, vol. 105, no. 4, pp. 1025–1102, 2005.
- [16] S. S. Shankar, S. Bhargava, and M. Sastry, "Synthesis of gold nanospheres and nanotriangles by the turkevich approach," *Journal of Nanoscience and Nanotechnology*, vol. 5, no. 10, pp. 1721–1727, 2005.
- [17] C.-H. Kuo, T.-F. Chiang, L.-J. Chen, and M. H. Huang, "Synthesis of highly faceted pentagonal- and hexagonal-shaped gold nanoparticles with controlled sizes by sodium dodecyl sulfate," *Langmuir*, vol. 20, no. 18, pp. 7820–7824, 2004.
- [18] J. A. Peck, C. D. Tait, B. I. Swanson, and G. E. Brown Jr., "Speciation of aqueous gold(III) chlorides from ultraviolet/visible absorption and Raman/resonance Raman spectroscopies," *Geochimica et Cosmochimica Acta*, vol. 55, no. 3, pp. 671–676, 1991.
- [19] D. V. Goia and E. Matijević, "Tailoring the particle size of monodispersed colloidal gold," *Colloids and Surfaces A: Physicochemical and Engineering Aspects*, vol. 146, pp. 139–152, 1999.



Hindawi

Submit your manuscripts at
<http://www.hindawi.com>

